Journal of Materials Chemistry A

Accepted Manuscript

ROYAL SOCIETY OF CHEMISTRY

www.rsc.org/materialsA

Phosphorus-Doped Carbon-Carbon Nanotube Hierarchical Monoliths as True Three-Dimensional Electrodes in Supercapacitor Cells

Julián Patiño, Nieves López-Salas, María C. Gutiérrez, Daniel Carriazo,[‡] M. Luisa Ferrer,[*] and Francisco del Monte[*]

Instituto de Ciencia de Materiales de Madrid-ICMM, Consejo Superior de Investigaciones Científicas-CSIC. Campus de Cantoblanco, 28049-Madrid (Spain)

[‡] Current address: *CIC Energigune, Parque Tecnológico de Álava. Albert Einstein, 48. 01510-Miñano* and *Ikerbasque, Basque Foundation for Science, 48011-Bilbao (Spain)*

* Address correspondence to mferrer@icmm.csic.es (M.L.F.) or delmonte@icmm.csic.es (F.dM.)

Abstract

Eutectic mixtures of the monohydrated form of *p*-toluenesulfonic acid (pTsOH·H_2O) and triethyl phosphate (TEP) in a 1:1 molar ratio were used as the medium to disperse previously-functionalized multiwalled carbon nanotubes (MWCNTs), and to catalyse the polycondensation of furfuryl alcohol. Hierarchically-structured P-doped carbon-CNT composites were obtained after carbonization. The high surface area and the phosphate functionalization, besides the hierarchical structure and good electrical conductivity exhibited by these composites provided remarkable metrics when they were used as electrodes in a supercapacitor cell, with energy densities of around 22.6 W h kg^{-1} at power densities of up to 10 kW kg^{-1} for operational voltages of up to 1.5 V. This performance surpasses any performance previously reported for electrodes weighing (at least) 10 mg per cm^2 of current collector and using an aqueous electrolyte. Actually, the supercapacitor cell built up with these electrodes provided enough neat energy to turn an IR LED of 30 mW on and emit light over a certain time.

Introduction

Supercapacitors, pseudo-capacitors and batteries – e.g. lithium and sodium ion batteries, and the most recent lithium–sulfur and metal–air ones – are attracting great attention because of the increasing demand of energy storage systems.[1, 2, 3, 4, 5, 6, 7, 8] Pseudo-capacitors and batteries store energy through a Faradic process – involving fast and reversible redox reactions between electrolyte and electro-active materials on the electrode surface.[9] Meanwhile, supercapacitors – or electrochemical double-layer capacitors (EDLCs) – store energy as a build-up of charge in the layers of the electrical double-layer formed at the interface between a high-surface area electrode and the adsorbed anions and cations of the electrolyte offering an enhanced rate capability, pulse power supply, long cycle life, and high dynamics of charge propagation as compared to pseudo-capacitors and batteries.[10, 11] The use of porous carbons – with high specific surface area, pores diameter matching the ions size, and good electrical conductivity – as electrodes in EDLCs has provided outstanding performances in terms of both energy and power densities.[12, 13] Within the context of porous-carbon-based electrodes, carbon aerogels with a three dimensional (3D) hierarchical porous structure (combining micro-, meso- and/or macropores) have attracted an increased attention as electrode materials for EDLCs because meso- and macropores may enhance the dynamic charge propagation by facilitating ions diffusion to the inner surfaces or even providing ion buffering reservoirs that minimize the diffusion distances.[14, 15, 16, 17, 18]

The use of carbon nanotubes (CNTs) and graphene has further improved the performance of the resulting electrodes.[19, 20, 21, 22, 23] Thus, Ragone plots providing energy densities approaching or even exceeding those of batteries while preserving good cyclability and power density have been described for some remarkable EDLCs. However, some of these results should be taken with caution if one desires to extrapolate these lab results to the industrial scale. The problem resides in the discrepancy between the dimensions and densities of the electrodes used for publication purposes and those of commercial electrodes. Actually, some critical works recently published by Gogotsi and Simon, and Ruoff and coworkers revealed that despite the remarkable metrics reported for many electrodes, the ultimate performance of a hypothetic device built up with them might be rather mediocre.[24, 25] Thus, they indicated that extrapolation is only valid for electrodes weighing (at least) 10 mg per cm^2 of current collector. Otherwise, there may be a significant drop in the capacitance when one needs to increase the thickness of the porous carbon electrode. Unfortunately, there are few works providing information in this regard and, among them, it is worth noting that this figure is below 3-5 mg/cm^2 in most of them,[26, 27, 28, 29, 30, 31, 32, 33, 34, 35, 36, 37, 38, 39, 40, 41, 42, 43, 44, 45, 46, 47, 48, 49, 50, 51] within the 5-10 mg/cm^2 range in just some few ones,[52, 53, 54, 55, 56, 57, 58, 59] and quite rarely

above 10 mg/cm^2. [60, 61, 62, 63, 64, 65, 66, 67, 68, 69] A close inspection to these works allows corroborating what Gogotsi and Simon previously stated. For instance, Ruoff and coworkers have recently described how the energy and power density performance of highly porous graphene-derived carbons drops, respectively, from □74 Wh kg^{-1} and 338 kW kg^{-1} to □55 Wh kg^{-1} and 23 kW kg^{-1} when the electrode mass loading increases from 1.3 mg/cm^2 (for a film thickness of □45 μm) to 10.4 mg/cm^2 (for a film thickness of □275 μm). Interestingly, this situation occurred even though these materials were synthesized in form of hierarchical pore structures that combined both mesopores and macropores.[50] Moreover, Gogotsi and Simon's statement seems to apply not only when mass loadings are near the threshold value of 10 mg/cm^2 but also in the whole range of mass loadings. For instance, the extraordinary power densities provided by graphene/MnO_2 composites[31] were clearly surpassed – more than 5-fold – by those provided by CNT/MnO_2.[30] There may be many reasons to explain this behaviour – e.g., electrode composition (graphene versus CNT), electrolyte (KOH versus Na_2SO_4), among others – but it is worth noting that the mass loading was 0.4 mg/cm^2 in the former case and only 0.03 mg/cm^2 in the latter one. In view of all these results, we think the preparation of electrodes capable to provide good performances and weighing more than 10 mg per cm^2 of current collector is yet challenging.

We have recently described the preparation of monolithic carbons and carbon-CNT composites using deep eutectic solvents (DESs). [68, 69, 70, 71, 72, 73] DESs – first described by Abbott and coworkers in 2003[74, 75, 76, 77] – are molecular complexes typically formed between quaternary ammonium salts – e.g. choline chloride or tetraethylammonium chloride – and hydrogen-bond donors. The charge delocalization occurring through hydrogen bonding between the halide anion and the hydrogen-donor moiety is responsible for the decrease of the freezing point of the mixture relative to the melting points of the individual components. DESs are considered a sub-group within conventional ionic liquids (ILs) as they actually share many properties (e.g. non-reactive with water and non-volatile, among others). However, they offer certain advantages as carbon precursors because of their greenness features.[78] In addition, DES-assisted polycondensations result in the direct – without the use of any further structure directing agent – formation of monolithic carbons built of highly cross-linked clusters that aggregated and assembled into a stiff and interconnected hierarchical structure. Among them and as electrodes in supercapacitor cells, monolithic carbon-CNT composites provided a remarkable performance in terms of power density – considering they were used as monolithic cylinders of 12 mm in diameter and 1 mm in height.[69] Unfortunately, the performance was not remarkable in terms of energy density because CNTs contribution to supercapacity was negligible – they could just be considered as inert mass in supercapacitive terms.[79] Meanwhile,

the use of phosphate-functionalized carbon materials as electrodes in supercapacitor cells opened interesting perspectives because they allow widening the typically narrow operational voltage window of aqueous electrolytes – up to 1.5-1.6 volts – and hence, improve the energy density that can be attained.[68, 80]

Herein, we have prepared phosphorus-doped carbon-CNT composites with the aim of obtaining good performances in terms of both energy and power density. For this purpose, CNTs were homogeneously dispersed in an eutectic mixture formed with the monohydrated form of *p*-toluenesulfonic acid (pTsOH·H_2O) and triethyl phosphate (TEP) in a 1:1 molar ratio, where pTsOH catalyzed the polycondensation of furfuryl alcohol and TEP provided phosphate functionalities to the carbon resulting after thermal treatment at 800°C in a nitrogen atmosphere. The resulting P-doped carbon-CNT composites were processed in form of cylindrical monoliths of 12 mm in diameter and 1.5 mm in height and exhibited a hierarchical structure composed of macro and micropores. The supercapacitor cell was prepared upon the direct assembling of two monoliths without further processing. Each monolith weighted 32 mg so that our mass loading was 28.3 mg/cm^2, this is well above the minimum mass of electrode per cm^2 of current collector that, according to Gogotsi and Simon report, will allow a more realistic estimation of the performance of this particular electrode in a hypothetic commercial device.

Results and Discussion

The formation of the DES was accomplished by direct mixing of pTsOH·H_2O and TEP in a 1:1 molar ratio. The liquid nature of the resulting mixture is depicted in Fig. 1. Neither melting temperature (T_m) nor crystallization temperature (T_c) was displayed in the DSC scan (Fig. 1), a common feature observed for noneasily crystallizable ILs and DESs.[81] The formation of DES was also confirmed by ^{1}H NMR spectroscopy as revealed by the up-field chemical shift of the signals of the components in the DES as compared to those of the bare components (Fig. S1 and Table S1).[82, 83]

Multiwalled carbon nanotubes (MWCNTs) – previously purified and functionalized upon HNO_3 treatment – were easily suspended within the resulting DES – 0.05 g of MWCNT in 1 g of DES, see experimental part – thanks to the excellent solvent properties and low viscosity of the pTsOH·H_2O/TEP eutectic mixture. Upon furfuryl alcohol addition, polycondensation progressed by the catalytic action of pTsOH·H_2O – see FTIR and solid-state ^{13}C NMR spectra in Fig. S2 and S3, and Table S2 at supporting information for further information about this regard. Interestingly, the certain acidic nature that the MWCNTs surface gained upon functionalization promoted the preferential formation of highly cross-linked colloidal clusters

on the MWCNTs surface. After carbonization, SEM and TEM micrographs revealed the formation of a fibrillar-like interconnected structure built up of MWCNTs coated by carbon colloids (Fig. 2). The CNT content at the resulting P-doped carbon-CNT composite was ca. 25 wt% as revealed by TGA experiments (Fig. S4). It is plausible that MWCNTs percolation was already occurring at the solution stage thanks to the pTsOH·H_2O/TEP-DES capability to suspend large quantities of MWCNTs in a homogeneous fashion. After polycondensation and carbonization, this percolated structure was preserved because of the above-mentioned formation of a carbon shell that coated every MWCNT and formed strong junctions between them (Fig. 2). This intimate contact among MWCNTs throughout the entire monolithic structure was confirmed by the excellent electrical conductivity measured by the four-probe method – e.g. 3.4 Scm^{-1}. The XRD pattern of the P-doped carbon-CNT composite further confirmed the presence of MWCNTs and the amorphous nature of the carbon resulting from furfuryl alcohol polycondensation and subsequent carbonization (Fig. S5).

The carbon shell that coats the scaffolding-structure formed by the MWCNTs also provided interesting features for the future application of the monoliths as electrodes in supercapacitor cells. For instance, the nitrogen adsorption-desorption isotherm shown in Fig. 3a revealed a high surface area for this composite – e.g. 937 m^2/g. The nitrogen adsorption–desorption isotherm was type I with a first increase in adsorption at low relative pressures characteristic of microporous materials, and a second one at relative pressures close to unity typically ascribed to capillar condensation in macropores. CO_2 adsorption–desorption isotherms also confirmed the presence of an extended microporous network throughout the sample (Fig. 3b). Table S3 summarizes the Brunauer-Emmett-Teller surface area, the micropore volume at $p/p_0 \approx 0.99$ and the micropore diameter – ca. 0.68-0.62 nm, as obtained from the application of the 2D-NLDFT-HS method to the N_2 adsorption data (see Fig. S6) and the Dubinin–Radushkevich equation to the CO_2 adsorption data. Meanwhile, the presence of TEP during carbonization introduced phosphate functionalities on the porous surface of the resulting carbons as revealed by EDX-SEM, total reflection X-ray fluorescence (TXRF), X-Ray Photoelectron spectroscopy (XPS), and solid-state ^{31}P NMR. The phosphorus content ranged 4.3-6.3 wt% – according to data coming from EDX-SEM, TXRF, and XPS, see Table S4 – and it was mainly in form of phosphate moieties – according to data coming from XPS and solid-state ^{31}P NMR, see Fig. 4.

These results revealed that both the composition – with phosphate functionalities – and the structure – with micropores providing high surface areas capable to accommodate protons and ions from aqueous electrolytes, and macropores that allow mass transport and accessibility to such a microporous surface – were promising for the use of these P-doped

carbon-CNT composites as electrodes in supercapacitors. As mentioned in the introduction, we were interested in using monoliths because they can be directly assembled – i.e. without any further processing, such as using polyvinylidene fluoride (PVDF) as a binder to form pellets and/or adding carbon black to improve the electrode electrical conductivity – into the supercapacitor cell. Thus, we used cylindrical monoliths of 12 mm in diameter and polished them to the desired thickness – e.g. 1.5 mm in height, see Fig. 5a. The achievement of parallel plane circular faces was required for the electrical contact with the current collectors in the supercapacitor cell. The performance of these monoliths as supercapacitor electrodes was evaluated by cyclic voltammetry and galvanostatic measurements using H_2SO_4 – 2 M in water – as electrolyte (Fig. 5b). The voltammogram characteristic of the electric double-layer (EDL) mechanism – i.e. with rectangular shape – was not observed in our case because of the pseudocapacitive contribution of phosphate moieties.[68, 80] Actually, rectangular shape voltammograms were observed in non-doped carbon-CNT composites exhibiting similar morphologies (Fig. S7).[68] The occurrence of pseudocapacitance in P-doped carbon-CNT composites was further confirmed by the voltammogram obtained in a three-electrode electrochemical cell (Fig. S7). Interestingly, the upper range of the voltage window reached 1.5 V (Fig. 5b), this is well above the theoretical decomposition potential of water – e.g. 1.23 V. This feature has been ascribed to the blockage of non-stable but electrochemically active oxidation sites – e.g., quinone groups – by phosphate groups so that deterioration processes associated with free oxygen atoms are minimized. [68, 80] This pseudocapacitive behaviour was finally observed at the galvanostatic charge/discharge plot (Fig. 5d) since it deviated from the quasy-linear voltage increase/decrease at the charge/discharge cycle that is compatible with the EDL mechanism.[17]

This widening of the operational voltage window determined that the specific capacitance (C_{esp}, normalized by the mass of the carbon monolith) experienced a significant enhancement as compared to our previous results found for non-doped carbon-CNT composites also processed in form of monoliths – i.e. 220 F g^{-1} for P-doped carbon-CNT composites (Fig. 5c) versus ca. 100 F g^{-1} for non-doped ones, measured at 300 mA g^{-1} in both cases.[68] Interestingly, the percentage of this original capacitance that was retained at high current densities was remarkable – e.g. 75 F g^{-1} at 40 A g^{-1} (Fig. 5c). This combination of high capacitances and good capacitance retention at high current densities provided remarkable metrics at the Ragone plot with energy densities of around 22.6 W h kg^{-1} at power densities of up to 10 kW kg^{-1} (Fig. 5f). Interestingly, volumetric figures obtained from the gravimetric ones and the specific gravity of the sample – ca. 0.18 g cm^{-3} – were also good, with energy densities of around 4.1 W h dm^{-3} at power densities of up to 1.8 kW dm^{-3}. Moreover, capacitance fading

was less than 17 % after more than 10000 cycles even though the entire experiment was performed in heavy regime conditions – e.g. 0-1.5 V and 2.5 A g^{-1} (Fig. 5e).

We further studied the pseudocapacitive properties and charge storage kinetics of P-doped carbon-CNT composites by electrochemical impedance spectroscopy (EIS). Fig. 6a shows the Nyquist plots of P-doped carbon-CNT composites measured at different cell voltages. The plots consist of a small semi-circle at high frequencies followed by a vertical line –90° in an ideal capacitor – in the low frequency one. At the high-frequency region, the first intersection between the plot and the X-axis is related to the electrolyte resistance, and contact resistance between the working electrode and the current collector (R_s) whereas the second one is related to the internal resistance of the electrode (R_p). Thus, the diameter of the semi-circle (R_p – R_s) corresponds to the equivalent series resistance (ESR) of the electrodes and determines the power capability – i.e. charge/discharge rate – of the supercapacitor. In our case and considering we used electrodes in monolithic form, the R_s was remarkably low – ca. 380 mΩ – and revealed an intimate contact between the monoliths and the current collector when assembled into the capacitor cell[68] and how the porous structure of P-doped carbon-CNT composites facilitated the efficient access of electrolyte ions to the electroactive surface and shortened the ion diffusion path.[84, 85] The ESR value obtained for cell voltages within the 0-0.6 V range was ca. 313 mΩ, and increased to ca. 442 and 667 mΩ for cell voltages of 0.9 and 1.2 V, respectively. This trend has been ascribed to ion blocking effects taking place at high charging voltage because of the production of a remarkable large number of separated charge species.[86] However, the occurrence of ion blocking in our case should be taken with caution considering that we are using an aqueous electrolyte rather than a gel polymer one. It is therefore more plausible that our semi-circle was associated to the presence of faradaic pseudocapacitive interactions – the larger the semi-circle, the greater the pseudocapacitive interaction. This behaviour was actually observed in other heteroatom doped carbons – e.g. nitrogen ones – also exhibiting pseudocapacitance.[87] Interestingly, none semi-circle was observed at the Nyquist plot of non-doped carbon-CNT composites behaving as regular EDLCs (Fig. S8). Fig. 6a also shows how, at low frequencies, the imaginary part of the impedance spectra of P-doped carbon-CNT composites deviated from the 90° vertical line of ideal capacitors, hence indicating the non-ideal features of ours. Nonetheless, it is worth noting that inclined Nyquist curves can also be found in samples with pores of different sizes – e.g. from micro- to meso- up to macropores.[87] Actually, Nyquist plots inclined at low frequencies were also found in non-doped carbon-CNT composites behaving as regular EDLCs but with textural properties that resemble those of P-doped carbon-CNT ones (Fig. S8).[69]

Finally, Fig. 6b shows the Bode |Z| and phase angle plots of P-doped carbon-CNT

composites measured at different cell voltages. These plots display the changes of absolute impedance (|Z|) and phase angle (φ) as a function of frequency (f). At high frequency region, |Z| was almost independent of f whereas at the low-frequency region experienced a significant increase – the higher the cell voltage, the larger the increase – that was typically ascribed to non-homogeneous diffusion in the less-accessible sites.[88] Meanwhile and with regard to the φ plot, it is well known that all capacitors show resistive behaviour at high frequencies and capacitive behavior at low frequencies when φ approaches –90°.[89] The capacitor response times (τ_0) can be calculated from the frecuency when φ = –45° (f_0),[90, 91] this is the frecuency at which the resistive and capacitive impedances are equal. In our case and for a cell voltage of 0.9 V, φ reached a minimum at low frequencies of ca. –73° – in range to pervious φ reported for carbon-based pseudocapacitors[92] and farther to –90° than that of non-doped carbon-CNT composites (Fig. S8) – while τ_0 was ca. 11.4 seconds. In this regard, some of the more important factors that can influence the kinetic response of a supercapacitor are the ionic conductivity of the electrolyte, the surface area of carbon, the electronic conductivity, and the occurrence of pseudocapacitive reactions. However, electrode thickness – even for thickness of just some few micrometers and below – is also an important factor typically determining slow kinetics.[91, 93] Actually, response times within the some-few-seconds range have already been described for porous carbon monoliths working as EDLCs.[17] Interestingly, τ_0 in non-doped carbon-CNT composites exhibiting similar porous morphologies was ca. 2.4 seconds (Fig. S8), revealing the relevance of both pseudocapacitance and porous structure in the kinetic response of P-doped carbon-CNT composites.

It is worth noting that one may find in the literature metrics that are more remarkable than ours (see some of the works included in Table 1). However, the straightforward comparison of these data should be taken with caution. As mentioned in the introduction, the electrode performance in terms of power density is strongly dependent on the geometrical aspect of the electrode – e.g. thickness versus contact surface – that ultimately determines the electrode mass loading per area of the current collector.[24, 25] Actually, the most remarkable metrics in Table 1 always correspond to electrodes processed in form of thin films and with quite low mass loadings. However, the ultimate performance of a hypothetic device built up with this kind of electrodes might be rather mediocre because the energy stored in neat terms is low. Thus, powering a simple infrared light emitting diode (IR LED) of a remote control for TV would only be possible for some few of the electrodes described in the table, those capable of providing enough neat energy to turn the IR LED on and emit light over, at least, one single second – e.g. 30 mW (Table 2). Interestingly, our electrodes were not only among the electrodes capable to power the IR LED (Fig. 5f) but also provided the highest neat energy of all

of them – even though we were the only ones using aqueous electrolytes (Table 2). This result emphasized two particular features of our electrodes – high mass loadings and operational windows of up to 1.5 V for aqueous electrolytes – that make them suitable for real applications.

Conclusions

We have prepared a DES based upon the mixture of pTsOH·H_2O and TEP in a 1:1 molar ratio, the use of which as the medium to disperse previously-functionalized MWCNTs, and to catalyse the polycondenation of furfuryl alcohol resulted – after carbonization – in the formation of hierarchically-structured P-doped carbon-CNT composites. Interestingly, the monolithic form in which the composites can be processed allowed their direct assembly into the supercapacitor cell. The high surface area and the phosphorus functionalization, besides the hierarchical structure and good electrical conductivity exhibited by these composites provided remarkable metrics when they were used as electrodes, with energy densities of around 22.6 W h kg^{-1} at power densities of up to 10 kW kg^{-1} for operational voltages of up to 1.5 V. This performance surpasses any performance previously reported for electrodes weighing (at least) 10 mg per cm^2 of current collector and using aqueous electrolytes. It is obvious that much remarkable results have been provided for electrodes processed in form of thin films and weighing less than 3-5 mg per cm^2 of current collector but some of these results should be taken with caution if one desires to extrapolate lab results into real applications.

Experimental Part

Samples Preparation: DES was obtained upon thermal treatment (at 90 °C for 30 min) of the physical mixture of the individual components – e.g. pTsOH·H_2O and TEP – in a 1:1 molar ratio. MWCNTs were purified and functionalized upon thermal treatment (130 °C) in HNO_3 (14 M) over 6 h. The resulting MWCNTs (0.05 g) were suspended in the pTsOH·H_2O/TEP-DES (1 g) under vigorous stirring and overnight. Furfuryl alcohol (99.8 wt%, 0.2 g) was then added to the MWCNT/DES suspension. Homogenization was achieved by vortexing the suspension over 2 min. Polycondensation was carried out first at 37 °C over 8 h and then at 90 °C over 4 days in closed containers. The resulting monolithic resins were thermally treated at 800 °C over 4 h (the heating ramp was 1.0 °C min^{-1}) under a nitrogen atmosphere.

Samples characterization: ^{1}H NMR spectra were recorded in a Bruker spectrometer DRX-500. DESs were placed in capillary tubes, using deuterated chloroform ($CDCl_3$) as an external reference (the deuterium signal was used for locking and shimming the sample). FTIR spectra were recorded in a Bruker Model IFS60v. ^{13}C and ^{31}P solid-state NMR experiments were carried

out on a Bruker Advanced 400 MHz Wide Bore (9.39 T) spectrometer operating at 100.61 MHz for ^{13}C resonance and 161.97 MHz for ^{31}P resonance. A standard cross polarization pulse sequence was used for ^{13}C NMR spectra, with a ramp contact time of 3.5 ms, a ^{1}H 90° pulse width of 3 µs, a recycle delay of 4 s and acquisition time of 29 ms. Samples were spun at 10 kHz (MAS) in a 4-mm-diameter ZrO_2 rotor at room temperature. A total of 28000 scans were collected over a spectral width of 35 kHz. TPPM ^{1}H decoupling with a field strength of 80 kHz was applied during signal acquisition. Chemical shifts were reported relative to the external reference of CH_2 adamantine (29.5 ppm) relative to TMS. ^{31}P NMR spectra were acquired with a single pulse high power decoupling sequence – e.g. 90° pulse width of 4.8 µs, a recycle delay of 40 s and acquisition time of 29 ms. Samples were spun at 25 kHz (MAS) in a 2.5-mm-diameter ZrO_2 rotor with Vespel caps at room temperature. A total of 3500 scans were collected over a spectral width of 35 kHz. TPPM ^{1}H decoupling with a field strength of 55 kHz was applied during signal acquisition. Chemical shifts were reported relative to the external reference of ADP (0.8 ppm) relative to H_3PO_4 85%. XRD patterns were obtained in a Bruker D8 Advance diffractometer using CuKα radiation (0.05° step size, 3.5 s counting time). TXRF analysis was carried out in a S2 PicoFox spectrometer. X-Ray Photoelectron spectroscopy (XPS) surface analysis was performed in a VG ESCALAB 200R electron spectrometer equipped with a hemispherical electron analyser and an Al Kα (hυ = 1486.6 eV, 1 eV = $1.6302 \cdot 10^{-19}$ J) 120 watts X-ray source. Charge effects were corrected by taking the main C1s component at a binding energy (BE) of 284.8 eV. Nitrogen adsorption–desorption isotherms were measured at –196 °C using an ASAP 2020 from Micromeritics on samples previously degassed under dynamic vacuum (ca. 10^{-5} mbar) at 100 °C for 6 h. Brunauer-Emmett-Teller (BET) theory (based on the desorption branches of the isotherms) were used to calculate the specific surface areas (S_{BET}) of the materials. The total pore volume was determined at $p/p_0 \sim 0.99$, and the micropore volume was calculated using the Dubinin–Radushkevich (DR) equation. The PSD analysis in the full micro–mesopore range was performed using the new 2D-NLDFT-HS model assuming surface heterogeneity of pores with the data from both N_2 and CO_2 adsorption/desorption isotherm data.[94] The narrow microporosity was further assessed by CO_2 adsorption–desorption isotherms performed in a Micromeritics Tristar 3020 instrument, in the pressure range of 0.1–900 mbar and at 0 °C. With these data, micropore volumes and micropore diameters were also calculated using the Dubinin–Radushkevich (DR) equation for the carbon materials. The morphology of the resulting monoliths was studied by scanning electron microscopy (SEM, using a SEM Hitachi S-3000N) and transmission electron microscopy (TEM, with a JEOL-2000 system operating at 200 keV). The electrical conductivity (σ_{DC}) of the monoliths was measured by using a digital multimeter Fluke 8840A in a four-probe configuration. Two monoliths (of 12

mm in diameter and 1.5 mm in height, and weighing 32 mg each) were assembled in Swagelok-type cells using 0.45-μm-thick PVDF membrane as separator. Electrochemical characterization was carried out in a PGSTAT30 Autolab potentiostat/galvanostat in a H_2SO_4 (2 M) aqueous electrolyte and two tantalum grids as current collectors. The specific capacitance (C_{sp}) was obtained from the galvanostatic plots recorded at different current densities, using the current intensity (I), the voltage range (ΔV_c), the discharge time (Δt_c), and the mass of the active material in one electrode (m) for the calculation:

$$C_{sp} = \frac{2 \cdot I \cdot \Delta t_c}{\Delta V_c \cdot m} .$$

The power density – P – and the energy density – E – were obtained using the following expressions:

$$E_{sp} = \frac{C_{sp} \cdot V_{max}^2}{8 \cdot 3.6} .$$

$$P_{sp} = \frac{I \cdot \Delta V_c}{4 \cdot m} .$$

where V_{max} was the voltage used for the measurement. Volumetric results were obtained multiplying gravimetric ones by the density of the materials – e.g. 0.18 g cm^{-3}.

Acknowledgments

This work was supported by MINECO (MAT2012-34811). J. P. and N. L.-S. acknowledge MINECO for their respective FPI contracts. Dr. Conchi Ania and Prof. José Luís G. Fierro are acknowledged for helpful assistance with surface area and XPS measurements, respectively.

References

1 J.-M. Tarascon and M. Armand, "Issues and challenges facing rechargeable lithium batteries" *Nature* **2001**, *414*, 359–367

2 M. Armand and J.-M. Tarascon, "Building better batteries" *Nature* **2008**, *451*, 652–657

3 A. S. Arico, P. Bruce, B. Scrosati, J.-M. Tarascon, and W. Van Schalkwijk, "Nanostructured materials for advanced energy conversion and storage devices" *Nature Mater.* **2005**, *4*, 366–377

4 X. Ji, K. Y. Lee, and L. F. Nazar, "A highly ordered nanostructured carbon-sulphur cathode for lithium-sulphur batteries" *Nature Mater.* **2009**, *8*, 500–506

5 G. Girishkumar, B. McCloskey, A. C. Luntz, S. Swanson, and W. Wilcke, "Lithium-air battery: Promise and challenges" *J. Phys. Chem. Lett.* **2010**, *1*, 2193–2203

6 B. Dunn, H. Kamath, and J.-M. Tarascon, "Electrical energy storage for the grid: A battery of choices" *Science* **2011**, *334*, 928–935

[7] P. Simon and Y. Gogotsi, "Materials for electrochemical capacitors" *Nature Mater.* **2008**, *7*, 845–854

[8] P. Simon, Y. Gogotsi, and B. Dunn, "Where do batteries end and supercapacitors begin?" *Science* **2014**, *343*, 1210–211.

[9] E. Frackowiak, V. Khomenko, K. Jurewicz, K. Lota, and F. Béguin, "Supercapacitors based on conducting polymers/nanotubes composites" *J. Power Sources* **2006**, *2*, 413–418

[10] J. Chmiola, G. Yushin, Y. Gogotsi, C. Portet, P. Simon, and P. L. Taberna, "Anomalous Increase in Carbon Capacitance at Pore Sizes Less Than 1 Nanometer" *Science* **2006**, *313*, 1760–1763

[11] E. Raymundo-Piñero, K. Kierzek, J. Machnikowski, and F. Béguin, "Relationship between the nanoporous texture of activated carbons and their capacitance properties in different electrolytes" *Carbon* **2006**, *44*, 2498–2507

[12] E. Frackowiak, V. Presser, A. Balducci, and F. Béguin, "Carbons and electrolytes for advanced supercapacitors" *Adv. Mater.* **2014**, *26*, 2219–2251

[13] D. Hulicova-Jurcakova, M. Seredych, G. Q. Lu, and T. J. Bandosz, "Combined effect of nitrogen- and oxygen-containing functional groups of microporous activated carbon on its electrochemical performance in supercapacitors" *Adv. Funct. Mater.* **2009**, *19*, 438–447

[14] K. Xia, Q. Gao, J. Jiang, and J. Hu, "Hierarchical porous carbons with controlled micropores and mesopores for supercapacitor electrode materials" *Carbon* **2008**, *46*, 1718–1726

[15] Y. Zhai, Y. Dou, D. Zhao, P. F. Fulvio, R. T. Mayes, and S. Dai, "Carbon materials for chemical capacitive energy storage" *Adv. Mater.* **2011**, *23*, 4828–4850

[16] M. C. Gutiérrez, F. Picó, F. Rubio, J. M. Amarilla, F. J. Palomares, M. L. Ferrer, and F. del Monte, J. M. Rojo, "PPO_{15}-PEO_{22}-PPO_{15} block copolymer assisted synthesis of monolithic macro- and microporous carbon aerogels exhibiting high conductivity and remarkable capacitance" *J. Mater. Chem.* **2009**, *19*, 773–780.

[17] D. Carriazo, F. Picó, M. C. Gutiérrez, F. Rubio, J. M. Rojo, and F. del Monte, "Block-Copolymer assisted synthesis of hierarchical carbon monoliths suitable as supercapacitor electrodes" *J. Mater. Chem.* **2010**, *20*, 773–780.

[18] W. Xing, S. Z. Qiao, R. G. Ding, F. Li, G. Q. Lu, Z. F. Yan, and H. M. Cheng, "Superior electric double layer capacitors using ordered mesoporous carbons" *Carbon* **2006**, *44*, 216–224

[19] E. Frackowiak and F. Béguin, "Electrochemical storage of energy in carbon nanotubes and nanostructured carbons" *Carbon* **2002**, *40*, 1775–1787

[20] M. Kaempgen, C. K. Chan, J. Ma, Y. Cui, and G. Gruner, "Printable thin film supercapacitors using single-walled carbon nanotubes" *Nano Lett.* **2009**, *9*, 1872–1876

[21] Z.-S. Wu, Y. Sun, Y.-Z. Tan, S. Yang, X. Feng, and K. Müllen, "Three-dimensional graphene-based macro- and mesoporous frameworks for high-performance electrochemical capacitive energy storage" *J. Am. Chem. Soc.* **2012**, *134*, 19532–19535

[22] Y. Zhu, S. Murali, M. D. Stoller, K. J. Ganesh, W. Cai, P. J. Ferreira, A. Pirkle, R. M. Wallace, K. A. Cychosz, M. Thommes, D. Su, E. A. Stach, and R. S. Ruoff, "Carbon-based supercapacitors produced by activation of graphene" *Science* **2011**, *332*, 1537–1541

[23] Q. Wu, Y. Xu, A. Liu, and G. Shi, "Supercapacitors based on flexible graphene/polyaniline nanofiber composite films" *ACS Nano* **2010**, *4*, 1963–1970

[24] Y. Gogotsi and P. Simon, "True performance metrics in electrochemical energy storage" *Science* **2011**, *334*, 917–918

[25] M. D. Stoller and R. S. Ruoff, "Best practice methods for determining an electrode material's performance for ultracapacitors" *Energy Environ. Sci.* **2010**, *3*, 1294–1301

[26] D.-W. Wang, F. Li, M. Liu, G. Q. Lu, and H.-M. Cheng, "3D Aperiodic Hierarchical Porous Graphitic Carbon Material for High-Rate Electrochemical Capacitive Energy Storage" *Angew. Chem.* **2008**, *47*, 373–376.

[27] E. Raymundo-Piñero, F. Leroux, and F. Béguin, "A High-Performance Carbon for Supercapacitors Obtained by Carbonization of a Seaweed Biopolymer" *Adv. Mater.* **2006**, *18*, 1877–1882

[28] V. Khomenko, E. Raymundo-Piñero, and F. Béguin, "High-energy density graphite/AC capacitor in organic electrolyte" *J. Power Sources* **2008**, *177*, 643–651.

[29] C. Liu, Z. Yu, D. Neff, A. Zhamu, and B. Z. Jang, "Graphene-Based Supercapacitor with an Ultrahigh Energy Density" *Nano Lett.* **2010**, *10*, 4863–4868

[30] W. Chen, R. B. Rakhi, L. Hu, X. Xie, Y. Cui, and H. N. Alshareef, "High-Performance Nanostructured Supercapacitors on a Sponge" *Nano Lett.* **2011**, *11*, 5165–5172

[31] Y. He, W. Chen, X. Li, Z. Zhang, J. Fu, C. Zhao, and E. Xie, "Freestanding Three-Dimensional Graphene/MnO2 Composite Networks As Ultralight and Flexible Supercapacitor Electrodes" *ACS Nano* **2013**, *7*, 174–182

[32] Y. Han, S. Liu, D Li, and X. Li, "Three-dimensionally Hierarchical Porous Carbon Creating High-performance Electrochemical Capacitors" *Electrochim. Acta* **2014**, *138*, 193–199

[33] S. He, and W. Chen, "High performance supercapacitors based on three-dimensional ultralight flexible manganese oxide nanosheets/carbon foam composites" *J. Power Sources* **2014**, *262*, 391–400

[34] Z. Zhang, Z. Zhou, H. Peng, Y. Qin, and G. Li, "Nitrogen- and oxygen-containing hierarchical porous carbon frameworks for high-performance supercapacitors" *Electrochim. Acta* **2014**, *134*, 471–477

[35] J. Zhang, D. Yang, W. Li, Y. Gao, and H. Li, "Synthesis and electrochemical performance of porous carbons by carbonization of self-assembled polymer bricks" *Electrochim. Acta* **2014**, *130*, 699–706

[36] Y. Guo, Z. Shi, M. Chen, and C. Wang, "Hierarchical porous carbon derived from sulfonated pitch for electrical double layer capacitors" *J. Power Sources* **2014**, *252*, 235–243

[37] M. Oschatz, S. Boukhalfa, W. Nickel, J. T. Lee, S. Klosz, L. Borchardt, A. Eychmüller, G. Yushin, and S. Kaskel, "Kroll-carbons based on silica and alumina templates as high-rate electrode materials in electrochemical double-layer capacitors" *J. Mater. Chem. A* **2014**, *2*, 5131–5139

[38] Q. Wang, J. Yan, Y. Wang, T. Wei, M. Zhang, X. Jing, and Z. Fan, "Three-dimensional flower-like and hierarchical porous carbon materials as high-rate performance electrodes for supercapacitors" *Carbon* **2014**, *67*, 119–127

[39] M. Sun, G. Wang, X. Li, and C. Li, "Irradiation preparation of reduced graphene oxide/carbon nanotube composites for high-performance supercapacitors" *J. Power Sources* **2014**, *245*, 436–444

[40] Q. Wang, J. Yan, Y. Xiao, T. Wei, Z. Fan, M. Zhang, and X. Jing, "Interconnected porous and nitrogen-doped carbon network for supercapacitors with high rate capability and energy density" *Electrochim. Acta* **2013**, *114*, 165–172

[41] Y. S. Yun, C. Im, H. H. Park, I. Hwang, Y. Tak, and H.-J. Jin, "Hierarchically porous carbon nanofibers containing numerous heteroatoms for supercapacitors" *J. Power Sources* **2013**, *234*, 285–291

[42] T. Chou, C. Huang, R. Doong, and C. Hu, "Architectural design of hierarchically ordered porous carbons for high-rate electrochemical capacitors" *J. Mater. Chem. A* **2013**, *1*, 2886–2895

[43] Z. Lei, Z. Liu, H. Wang, X. Sun, L. Lu, and X. S. Zhao, "A high-energy-density supercapacitor with graphene–CMK-5 as the electrode and ionic liquid as the electrolyte" *J. Mater. Chem. A* **2013**, *1*, 2313–2321

[44] C.-M. Chen, Q. Zhang, X.-C. Zhao, B. Zhang, Q.-Q. Kong, M.-G. Yang, Q.-H. Yang, M.-Z. Wang, Y.-G. Yang, R. Schlögl, and D. S. Su, "Hierarchically aminated graphene honeycombs for electrochemical capacitive energy storage" *J. Mater. Chem.* **2012**, *22*, 14076–14084

[45] M. Yu, Y. Ma, J. Liu, and S. Li, "Polyaniline nanocone arrays synthesized on threedimensional graphene network by electrodeposition for supercapacitor electrodes" *Carbon* **2015**, *87*, 98–195

[46] X. Huang, Q. Wang, X. Y. Chen, and Z. J. Zhang, "N-doped nanoporous carbons for the supercapacitor application by the template carbonization of glucose: The systematic comparison of different nitridation agents" *J. Electroanal. Chem.* **2015**, *748*, 23–33

[47] F. Gao, G. Shao, J. Qu, S. Lv, Y. Li, and M. Wu, "Tailoring of porous and nitrogen-rich carbons derived from hydrochar for high-performance supercapacitor electrodes" *Electrochim. Acta* **2015**, *155*, 201–208

[48] B. Chang, Y. Guo, Y. Li, H. Yin, S. Zhang, B. Yang, and X. Dong*, "Graphitized hierarchical porous carbon nanospheres: simultaneous activation/graphitization and superior supercapacitance performance" *J. Mater. Chem. A* **2015**, *3*, 9565–9577

[49] S. Shivakumara, B. Kishore, T. R. Penki, and N. Munichandraiah, "Symmetric Supercapacitor Based on Reduced Graphene Oxide in Non-Aqueous Electrolyte" *ECS Electrochem. Lett.* **2015**, *4*, A87–A89

[50] T. Kim, G. Jung, S. Yoo, K. S. Suh, and R. S. Ruoff, "Activated Graphene-Based Carbons as Supercapacitor Electrodes with Macro- and Mesopores" *ACS Nano* **2013**, *7*, 6899–6905

[51] K. Tao, P. Li, L. Kang, X. Li, Q. Zhou, L. Dong, and W. Liang, "Facile and low-cost combustion-synthesized amorphous mesoporous NiO/carbon as high mass-loading pseudocapacitor materials" *J. Power Sources* **2015**, *293*, 23–32

[52] Z. Lei, N. Christov, L. L. Zhang, and X. S. Zhao, "Mesoporous carbon nanospheres with an excellent electrocapacitive performance" *J. Mater. Chem.* **2011**, *21*, 2274–2281

[53] C. X. Guo and C. M. Li, "A self-assembled hierarchical nanostructure comprising carbon spheres and graphene nanosheets for enhanced supercapacitor performance" *Energy Environ. Sci.* **2011**, *4*, 4504–4507

[54] H. Fan, F. Ran, X. Zhang, H. Song, W. Jing, K. Shen, L. Kong, and L. Kang, "Easy fabrication and high electrochemical capacitive performance of hierarchical porous carbon by a method combining liquid-liquid phase separation and pyrolysis process" *Electrochim. Acta* **2014**, *138*, 367–375

[55] Y. Mun, C. Jo, T. Hyeon, J. Lee, K.-S. Ha, K.-W. Jun, S.-H. Lee, S.-W. Hong, H. I. Lee, S. Yoon, and J. Lee, "Simple synthesis of hierarchically structured partially graphitized carbon by emulsion/block-copolymer co-template method for high power supercapacitors" *Carbon* **2013**, *64*, 391–402

[56] Q. Wang, Q. Cao, X. Wang, B. Jing, H. Kuang, and L. Zhou, "Dual template method to prepare hierarchical porous carbon nanofibers for high-power supercapacitors" *J. Solid State Electrochem.* **2013**, *17*, 2731–2739

[57] K. L. Van Aken, C. R. Pérez, Y. Oh, M. Beidaghi, Y. J. Jeong, M. F. Islam, and Y. Gogotsi, "High rate capacitive performance of single-walled carbón nanotube aerogels" *Nano Energy* **2015**, *15*, 662–669

[58] H. Zhang, K. Wang, X. Zhang, H. Lin, X. Sun, C. Li and Y. Ma, "Self-generating graphene and porous nanocarbon composites for capacitive energy storage" *J. Mater. Chem. A* **2015**, *3*, 11277–11286

[59] Y. Li and D. Zhao, "Preparation of reduced graphite oxide with high volumetric capacitance in supercapacitors" *Chem. Commun.* **2015**, *51*, 5598–5601

[60] K. Kim, M. Choi, and R. Ryoo, "Ethanol-based synthesis of hierarchically porous carbon using nanocrystalline beta zeolite template for high-rate electrical double layer capacitor" *Carbon* **2013**, *60*, 175–185

[61] K. H. An, W. S. Kim, Y. S. Park, J.-M. Moon, D. J. Bae, S. C. Lim, Y. S. Lee, and Y. H. Lee, "Electrochemical Properties of High-Power Supercapacitors Using Single-Walled Carbon Nanotube Electrodes" *Adv. Funct. Mater.* **2001**, *11*, 387–392

[62] V. Ruiz, C. Blanco, R. Santamaría, J. M. Ramos-Fernández, M. Martínez-Escandell, A. Sepúlveda-Escribano, and F. Rodríguez-Reinoso, "An activated carbon monolith as an electrode material for supercapacitors" *Carbon* **2009**, *47*, 195–200

[63] M. Kunowsky, A. García-Gomez, V. Barranco, J. M. Rojo, J. Ibañez, J. D. Carruthers, and A. Linares-Solano, "Dense carbon monoliths for supercapacitors with outstanding volumetric capacitances" *Carbon* **2014**, *68*, 553–562

[64] H. Qian, A. R J Kucernak, E. S. Greenhalgh, A. Bismarck, and M. S. P. Shaffer, "Multifunctional structural supercapacitor composites based on carbon aerogel modified high performance carbon fibre fabric" *ACS Appl. Mater. Interfac.* **2013**, *5*, 6113–6122

[65] C. Zheng, W. Qian, C. Cui, Q. Zhang, Y. Jin, M. Zhao, P. Tan, and F. Wei ,"Hierarchical carbon nanotube membrane with high packing density and tunable porous structure for high voltage supercapacitors" *Carbon* **2012**, *50*, 5167–5175.

[66] A. Khosrozadeh, M. Xing, Q. Wang, "A high-capacitance solid-state supercapacitor based on free-standing film of polyaniline and carbon particles" *Appl. Energy* **2015**, *153*, 87–93

[67] M. Liu, J. Qian, Y. Zhao, D. Zhu, L. Gan, and L. Chen, "Core–shell ultramicroporous@microporous carbon nanospheres as advanced supercapacitor electrodes" *Carbon* **2012**, *50*, 5167–5175.

[68] D. Carriazo, M. C. Gutiérrez, F. Picó, J. M. Rojo, J. L. G. Fierro, M. L. Ferrer, and F. del Monte, "Phosphate-Functionalized Carbon Monoliths from Deep Eutectic Solvents and their Use as Monolithic Electrodes in Supercapacitors" *ChemSusChem* **2012**, *5*, 1405–1409.

[69] M. C. Gutiérrez, D. Carriazo, A. Tamayo, R. Jiménez, F. Picó, J. M. Rojo, M. L. Ferrer, and F. del Monte, "Deep-Eutectic-Solvent-Assisted Synthesis of Hierarchical Carbon Electrodes Exhibiting Capacitance Retention at High Current Densities" *Chem. Eur. J.* **2011**, *17*, 10533–10537.

[70] D. Carriazo, M. C. Gutiérrez, M. L. Ferrer, and F. del Monte, "Resorcinol-Based Deep Eutectic Solvents as Both Carbonaceous Precursors and Templating Agents in the Synthesis of Hierarchical Porous Carbon Monoliths" *Chem. Mater.* **2010**, *22*, 6146–6152.

[71] D. Carriazo, M. C. Gutiérrez, R. Jiménez, M. L. Ferrer, and F. del Monte, "Deep-Eutectic-Assisted Synthesis of Bimodal Porous Carbon Monoliths with High Electrical Conductivities" *Part. Part. Sys. Charact.* **2013**, *30*, 316–320.

[72] J. Patiño, M. C. Gutiérrez, D. Carriazo, C. O. Ania, J. L. Parra, M. L. Ferrer, and F. del Monte, "Deep eutectic assisted synthesis of carbon adsorbents highly suitable for low-pressure separation of CO_2–CH_4 gas mixtures" *Energy Environ. Sci.* **2012**, *5*, 8699–8707.

[73] For a recent review, see: D. Carriazo, M. C. Serrano, M. C. Gutiérrez, M. L. Ferrer, and F. del Monte, "Deep-eutectic solvents playing multiple roles in the synthesis of polymers and related materials" *Chem. Soc. Rev.* **2012**, *41*, 4996–5014.

[74] A. P. Abbott, G. Capper, D. L. Davies, R. K. Rasheed, and V. Tambyrajah, "Novel solvent properties of choline chloride/urea mixtures" *Chem. Commun.* **2003**, 70–71.

[75] A. P. Abbott, R. C. Harris, and K. S. Ryder, "Application of Hole Theory to Define Ionic Liquids by their Transport Properties" *J. Phys. Chem. B* **2007**, *111,* 4910–4913

[76] A. P. Abbott, G. Capper, and S. Gray, "Design of Improved Deep Eutectic Solvents Using Hole Theory" *ChemPhysChem* **2006**, *7,* 803–806.

[77] A. P. Abbott, D. Boothby, G. Capper, D. L. Davies, and R. K. Rasheed, "Deep Eutectic Solvents Formed between Choline Chloride and Carboxylic Acids: Versatile Alternatives to Ionic Liquids" *J. Am. Chem. Soc.* **2004**, *126,* 9142–9147.

[78] For a recent review, see: F. del Monte, D. Carriazo, M. C. Serrano, M. C. Gutiérrez, and M. L. Ferrer, "Deep Eutectic Solvents in Polymerizations: A Greener Alternative to Conventional Syntheses" *ChemSusChem* **2014**, *7*, 999 – 1009

[79] S. Roldán, C. Blanco, M. Granda, R. Menéndez, and R. Santamaría, "Towards a Further Generation of High-Energy Carbon-Based Capacitors by Using Redox-Active Electrolytes" *Angew. Chem.* **2011**, *50*, 1699 –1701

[80] D. Hulicova-Jurcakova, A. M. Puziy, O. I. Poddubnaya, F. Suarez-García, J. M. D. Tascon, and G.-Q. Lu, "Highly Stable Performance of Supercapacitors from Phosphorus-Enriched Carbons" *J. Am. Chem Soc.* **2009**, *131*, 5026–5027.

[81] W. Xu, E. I. Cooper, and C. A. Angell, "Ionic liquids: Ion mobilities, glass temperatures, and fragilities" *J. Phys. Chem. B* **2003**, *107*, 6170−6178.

[82] M. C. Gutiérrez, M. L. Ferrer, C. R. Mateo, F. del Monte, "Freeze-Drying of Aqueous Solutions of Deep Eutectic Solvents: A Suitable Approach to Deep Eutectic Suspensions of Self-Assembled Structures." *Langmuir*, **2009**, *25*, 5509–5515.

[83] M. C. Gutiérrez, M. L. Ferrer, L. Yuste, F. Rojo, F. del Monte, "Bacteria Incorporation in Deep-eutectic Solvents through Freeze-Drying." *Angew. Chem., Int. Ed.* **2010**, *49*, 2158–2162.

[84] A. S. Arico, P. Bruce, B. Scrosati, J.-M. Tarascon, and W. Van Schalkwijk, "Nanostructured materials for advanced energy conversion and storage devices" *Carbon* **2010**, *48*, 1731–1737

[85] S. T. Senthilkumar, R. Kalai Selvan, Y. S. Lee, and J. S. Melo, "Electric double layer capacitor and its improved specific capacitance using redox additive electrolyte" *J. Mater. Chem. A* **2013**, *1*, 1086–1095

[86] S. N. Syahidah, S. R. Majid, "Super-capacitive electro-chemical performance of polymer blend gel polymer electrolyte (GPE) in carbon-based electrical double-layercapacitors" *Electrochim. Acta* **2013**, *112*, 678–685

[87] D. Hulicova, M. Kodama, and H. Hatori, "Electrochemical Performance of Nitrogen-Enriched Carbons in Aqueous and Non-Aqueous Supercapacitors" *Chem. Mater.* **2006**, *18*, 2318–2326

[88] D. Yuan, J. Zeng, N. Kristian, Y. Wang, and X. Wang, "Bi_2O_3 deposited on highly ordered mesoporous carbon for supercapacitors" *Electrochem. Commun.* **2009**, *11*, 313–317

[89] D.-W. Wang, F. Li, H.-T. Fang, M. Liu, G.-Q. Lu, and H.-M. Cheng, "Effect of Pore Packing Defects in 2D Ordered Mesoporous Carbons on Ionic Transport" *J. Phys. Chem. B* **2006**, *110*, 8570–8575

[90] F. Lufrano and P. Staiti, "Performance improvement of Nafion based solid state electrochemical supercapacitor" *Electrochim. Acta* **2004**, *49*, 2683–2689

[91] F. Meng and Y. Ding, "Sub-Micrometer-Thick All-Solid-State Supercapacitors with High Power and Energy Densities" *Adv. Mater.* **2011**, *23*, 4098–4102

[92] L. Yuan, X.-H. Lu, X. Xiao, T. Zhai, J. Dai, F. Zhang, B. Hu, X. Wang, L. Gong, J. Chen, C. Hu, Y. Tong, J. Zhou, and Z. L. Wang, "Flexible Solid-State Supercapacitors Based on Carbon Nanoparticles/MnO_2 Nanorods Hybrid Structure" *ACS Nano* **2011**, *6*, 656–661

[93] K. Sheng, Y. Sun, C. Li, W. Yuan, and G. Shi, "Ultrahigh-rate supercapacitors based on eletrochemically reduced graphene oxide for ac line-filtering" *Sci. Reports.* **2012**, *2*, Article number: 247

[94] G. Rasines, C. Macías, M. Haro, J. Jagiello, C. O. Ania, "Effects of CO_2 activation of carbon aerogels leading to ultrahigh micro-meso porosity" *Micropor. Mesopor. Mat.* **2015**, *209*, 18–22

Table 1: Gravimetric data obtained from the Ragone plot of a set of supercapacitor cells that used different carbon materials as electrodes. Data with regard to some other aspects that may determine the performance of the different supercapacitor cells – e.g. the processing of the electrode, the mass loading of active material, the electrolyte, and the electrochemical window – are also included.

Ref	Type of Electrode - Processing	Mass of electrode per Area of current collector (mg cm^{-2})	Electrolyte	ΔV (V)	Gravimetric Data obtained from Ragone Plot	
					Highest E density ($W \cdot h \cdot Kg^{-1}$) P density ($kW \cdot Kg^{-1}$) at the highest E density is included between brackets	Highest P density ($kW \cdot Kg^{-1}$) E density ($W \cdot h \cdot Kg^{-1}$) at the highest P density is included between brackets
This work	Monolith – Directly assembled	32.0/1.13 = 28.3	2 M H_2SO_4 in H_2O	1.5	39.5 (0.02)	7.8 (12.5)
26	Slurry – Spread onto Ni foam	5.0/1.0 = 5.0	1.5 M $TEABF_4$ in Acetonitrile	2.5	22.9 (0.11)	23.0 (22.0)
26	Slurry – Spread onto Ni foam	5.0/1.0 = 5.0	6 M KOH in H_2O	1.0	9.5 (0.01)	25.0 (5.5)
26	Pellet – Directly assembled	5.0/1.0 = 5.0	6 M KOH in H_2O	1.0	10 (0.2)	4.0 (2.0)
27	Pellet – Directly assembled	0.37/1.0 = 0.37	1 M H_2SO_4 in H_2O	1.0	7.4 (0.06)	10.4 (4.0)
28	Pellet Hybrid– Directly assembled	2.08-6.24/1.04 = 2-6	1 M $LiPF_6$ in EC:DMC 1:1	5.0	145.8 (0.065)	10.0 (2.0)
28	Pellet Hybrid – Directly assembled	2.08-6.24/1.04 = 2-6	1 M $LiPF_6$ in EC:DMC 1:1	4.5	103.8 (--)	10.0 (--)
28	Pellet – Directly assembled	2.08-6.24/1.04 = 2-6	1 M $LiPF_6$ in EC:DMC 1:1	3.0	22.6 (0.11)	60.0 (2.0)
28	Pellet – Directly assembled	2.08-6.24/1.04 = 2-6	1 M $TEABF_4$ in Acetonitrile	2.5	22.6 (0.16)	18.0 (5.0)

29	Pellet – Directly assembled	6.6/1.33 = 4.97	$EMIMBF_4$	4.5	85.6 (0.55)	10.0 (50.0)
30	CNT MnO_2 Sponge – Elecrodeposited	0.03/1.0 = 0.03*	1 M Na_2SO_4 in H_2O	1.0	31 (65)	105 (--)
31	Graphene MnO_2 – Elecrodeposited onto Ni foam	0.4/1.0 = 0.4	0.5 M Na_2SO_4 in H_2O	1.0	6.8 (0.06)	2.5 (3.8)
32	Slurry – Spread onto Ni foam	3-5/1 = 3-5	6 M KOH in H_2O	1.0	17(0.24)*	2.4(12)*
33	Carbon MnO_2 Sponge – Directly assembled	1.0/87.5 = 0.012	1 M Na_2SO_4 in H_2O	0.7	86.2(0.2)	160(7)
34	Slurry – Spread onto steel mesh	1.178/0.785 = 1.5	1 M H_2SO_4 in H_2O	0.8	37.4(0.2)	18.6(14.3)
35	Slurry – Spread onto Ni foam	4/1 = 4	6 M KOH in H_2O	1.0	14.17*(0.1*)	4*(11.33*)
36	Slurry - Rolled	5.45/1.33 = 4.1*	6 M KOH in H_2O	1.0	10(0.01)	30(6)
36	Slurry - Rolled	5.45/1.33 = 4.1*	1M Li_2SO_4 in H_2O	1.6	20(0.08)	4(8)
36	Slurry - Rolled	5.45/1.33 = 4.1*	1 M $TEABF_4$ in PC	2.7	40(0.05)	1(10)
37	Slurry - Rolled	2-3/1 = 2-3	1 M H_2SO_4 in H_2O	0.6	6.5(0.1)	30(6)
37	Slurry - Rolled	2-3/1 = 2-3	EMINBF4	2.3	70(0.4)	90(60)
38	Slurry - Spread onto Ni foam	4.4/1 = 4.4*	1 M Na_2SO_4 in H_2O	1.8	15.9(0.3)	20(10)
39	Slurry – evaporates onto steel	0.2/2 = 0.1	1 M H_2SO_4 in H_2O	0.8	10.05*(0.2*)	20(7.78*)

40	Slurry – Spread onto Ni foam	1.6/1 = 1.6*	1 M Na_2SO_4 in H_2O	1.6	26(0.55)	30(12)
41	Pellet - Directly assembled	2.5-3/1 = 2.5-3	BMINBF4/AN (1:1)	3.0	250(3)	100(150)
41	Pellet - Directly assembled	2.5-3/1 = 2.5-3	1 M H_2SO_4 in H_2O	1.0	110(1)	10(30)
42	Slurry – Evaporated	0.9/1 = 0.9	4 M H_2SO_4 in H_2O	1.0	10(1)	10(4)
43	Slurry - Rolled	3	6 M KOH in H_2O	1.0	6(0.09)	4(0.6)
43	Slurry - Rolled	3	1 M $LiPF_6$ in EC:DMC 1:1	2.5	25(0.2)	7(2)
43	Slurry - Rolled	3	$EMIMBF_4$	3.5	60.7(0.17)	11(10)
44	Pellet - Directly assembled	3.5/0.8 = 4.375	6 M KOH in H_2O	1.0	7(0.08)	6(3)
45	PANI – Elecrodeposited onto graphene foam	4.75/2 = 2.375*	1 M $HClO_4$ in H_2O	0.7	16.1 (0.175)	1.75 (12.6)
46	Slurry – Spread onto Ni foam	2.5/1= 2.5	6 M KOH in H_2O	1.0	30 (0.5)	5 (10.1)
47	Slurry – Pressed on Ti mesh	3.5/1.77=1.97	1M H_2SO_4 in H_2O*	1.0	12 (0.2)	1.0 (6.2)
48	Slurry – Spread onto Ni foam	1-2/1.0=1-2	6M KOH in H_2O	1.0	54 (0.5)	30 (45)
49	Slurry – Spread onto stainless steel disk	3-4/2.01=1.5-2	1 M $LiPF_6$ in EC, DEC and DMC (2:1:2 v/v)	3.0	44 (0.1)	8 (15)
50	Pellet - Directly assembled	1.3/1 = 1.3	[EMIM][TFSI]/AN	3.5	74(338)	-- (--)
51	Slurry – Spread onto Ni foam	1.43	2 M KOH in H_2O	0.4	14.13 (0.1)	1.0 (7.1)
46	Slurry – Spread onto Ni foam	9.38	2 M KOH in H_2O	0.4	6.5 (0.1)	-- (--)

52	Slurry – Spread onto Ni foam	7.0/1.0 = 7.0	1.5 M $TEABF_4$ in Acetonitrile	3.0	62.8 (0.17)	32.0 (10.0)
52	Slurry – Spread onto Ni foam	7.0/1.0 = 7.0	6 M KOH in H_2O	1.0	7.7 (0.05)	8.6 (3.0)
52	Slurry – Spread onto Ni foam	7.0/1.0 = 7.0	1.5 M $TEABF_4$ in Acetonitrile	3.0	37.7 (0.15)	9.0 (10.0)
53	Slurry – Spread onto Ni foam	8.2/1.33 = 6.16	6 M KOH in H_2O	1.0	-- (--)	15.4(--)
54	Slurry – Spread onto Ni foam	8/1 = 8	2 M KOH in H_2O	1.0	4.69(0.31)	3.12(3.47)
55	Slurry – Spread onto steel	5.5/1 = 5.5*	2 M H_2SO_4 in H_2O	1.0	4(0.02)	1(3)
56	Slurry – Spread onto steel mesh	4-7/1 = 4-7	6 M KOH in H_2O	1.0	10(7.5)	15(5)
57	SWCNT Aerogel – Directly assembled	6*	EMI-TFSI	2.5	50 (0.7)	110 (11)
58	Slurry – Pressed on Al foil	8.8*/1.33=6.62*	$EMIMBF_4$	3.5	78 (1.0)	11 (40)
59	Slurry – Spread onto Ni foam	10/1 = 10	6 M KOH in H_2O	1	6.45* (0.25)*	2.5 (4.4)
60	Pellet - Directly assembled	8/0.78 = 10.26	1 M $TEABF_4$ in PC	2.5	20(0.05)	6(10)
61	Pellet – Directly assembled	19.9/1.77 = 11.25*	7.5 N KOH in H_2O	0.9	19.0 ($1.8 \cdot 10^{-3}$)	20.0 (7.5)
62	Monolith – Directly assembled	23.4/1.33 = 17.6	1 M H_2SO_4 in H_2O	1.0	12 ($9.5 \cdot 10^{-3}$)	12.0 (1.0)
63	Monolith – Directly assembled	105.5-130.2 /0.79= 133.9-164.8*	2 M H_2SO_4 in H_2O	1.0	32.0 ($4.7 \cdot 10^{-3}$)	0.16 (15.0)
63	Monolith – Directly assembled	82.2-101.1/0.79= 104.0-128.0*	2 M H_2SO_4 in H_2O	1.0	38.0 ($7 \cdot 10^{-3}$)	0.2 (11.0)

64	Monolith – Directly assembled	1000/44.2= 22.6*	EMITFSI	0.1	$1.23 \cdot 10^{-3}$ ($4.2 \cdot 10^{-4}$)	-- (--)
64	Monolith – Directly assembled	1348/59.5= 22.6*	PEGDGE/EMITFSI (90/10 wt%)	0.1	$0.84 \cdot 10^{-3}$ ($0.33 \cdot 10^{-4}$)	-- (--)
50	Pellet - Directly assembled	10.4/1 = 10.4	[EMIM][TFSI]/AN	3.5	55(23)	-- (--)
65	CNT Sponge - directly assembled	16/1.33 = 12.03	1 M $TEABF_4$ in PC	4.0	35(0.03)	3(15)
66	TCPs-PANI – Directly assembled	40/3 = 13.3	1 M H_2SO_4 in H_2O*	0.8	11 (0.28)	0.58 (1.7)
67	Slurry – Spread onto Ni foam	10/1.0=10	6M KOH in H_2O	1.0	10.5 (0.5)	14 (4.0)
68	Monolith – Directly assembled	65.4/ 0.79 = 82.8	2 M H_2SO_4 in H_2O	1.4	13.0 ($8 \cdot 10^{-3}$)	0.2 (6.0)
69	Monolith – Directly assembled	29.9/1.13 = 26.5	2 M H_2SO_4 in H_2O	1.0	3.8 ($8 \cdot 10^{-3}$)	7.0 (2.1)

* Data estimated from reported figures

Table 2: Selected electrodes with remarkable performances that, according to the neat energy calculated from the data provided in Table 1, would be either capable or not to power the IR LED depicted in Figure 5g. For the capable ones, the table includes how long the IR LED would be on according to its power consumption (30 mW).

Ref.	ΔV (V)	E density ($W \cdot h \cdot Kg^{-1}$)	Neat Energy (J)	Capable to power the IR LED (yes/no)	Time (seconds)
This work	1.5[a]	39.5	4.550	Yes	100
29	4.5[b]	85.6	2.034	Yes	67.8
30	1[a]	31	0.003	No	--
50	3.5[b]	74	0.346	Yes	68
61	0.9[a]	19	1.361	No	--
65	4[b]	35	2.016	Yes	67

[a] Aqueous electrolyte. [b] Organic electrolyte. See Table 1 for further details

Figure 1. Left: Picture of the liquid resulting from the mixture of pTsOH·H_2O and TEP in a 1:1 molar ratio. **Right:** DSC scans – both cooling and heating – taken at a rate of 5 °C/min of pTsOH·H_2O and TEP in a 1:1 molar ratio. The eutectic mixture displayed neither a melting point (T_m) nor a crystallization temperature (T_c).

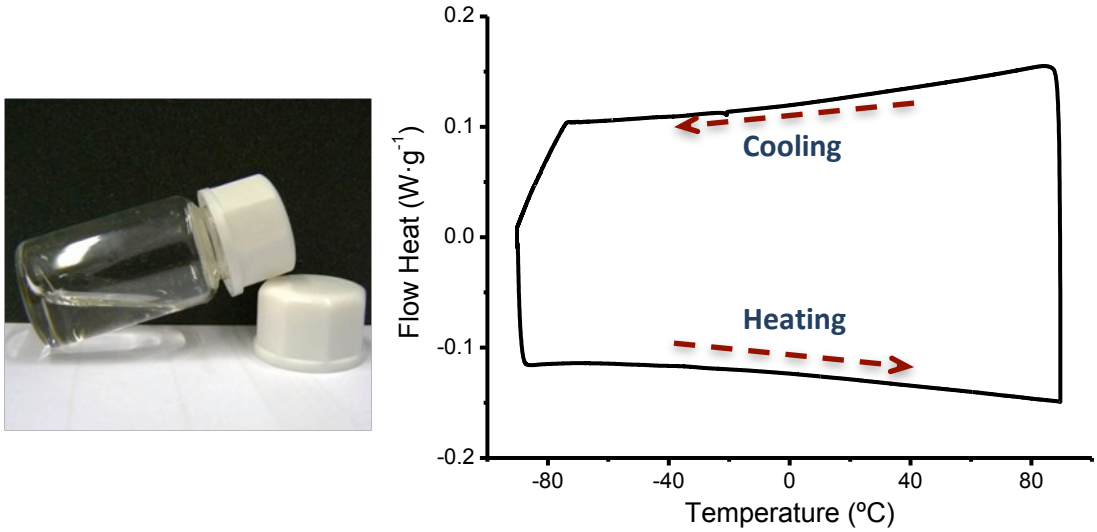

Figure 2. SEM (a, b and d) and TEM (c) micrographs of P-doped carbon-CNT composites.

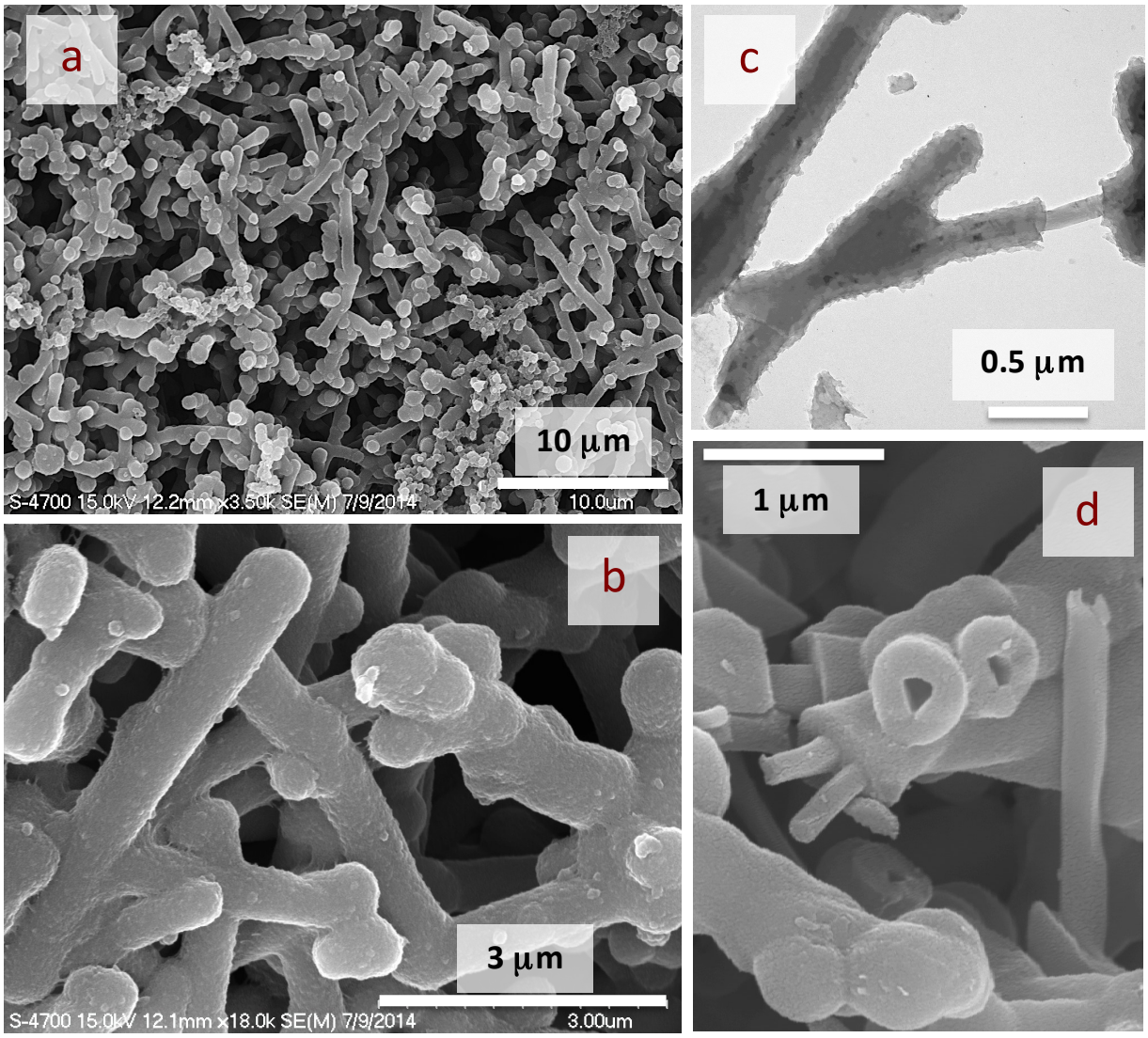

Figure 3. N_2 (a) and CO_2 (b) adsorption-desorption isotherms (at -196°C and 0°C, respectively) of P-doped carbon-CNT composites.

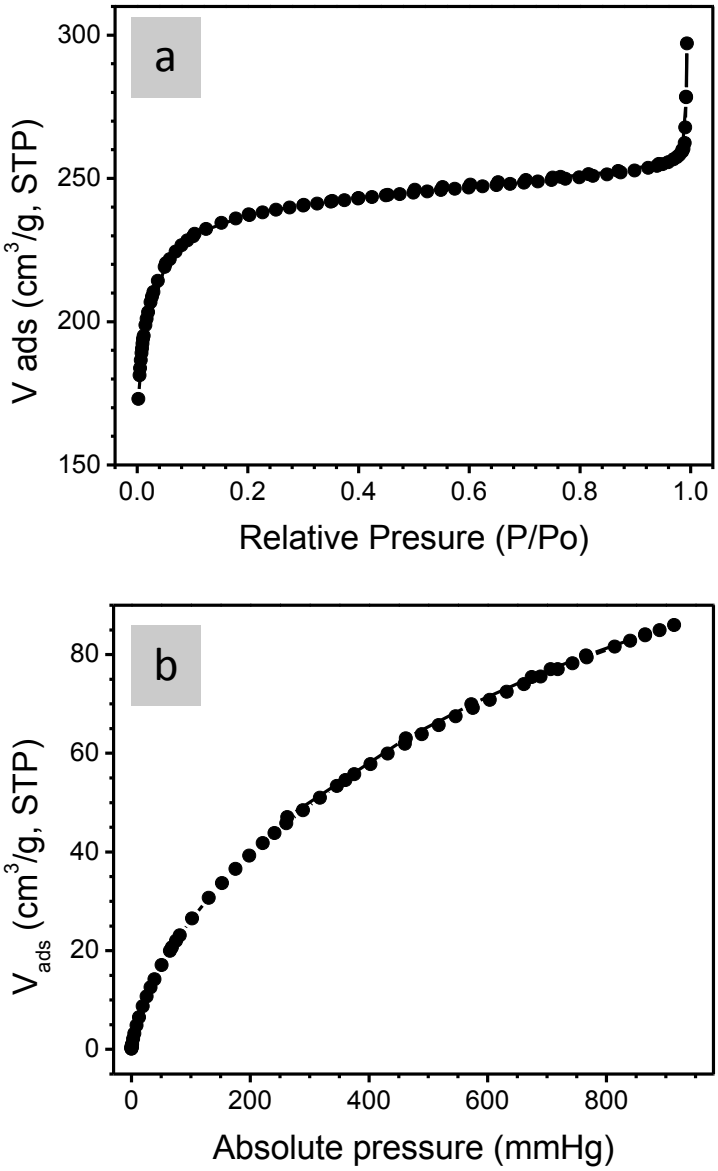

Figure 4. XPS P_{2p} core-level (top) and solid-state ^{31}P NMR (bottom) spectra of P-doped carbon-CNT composites.

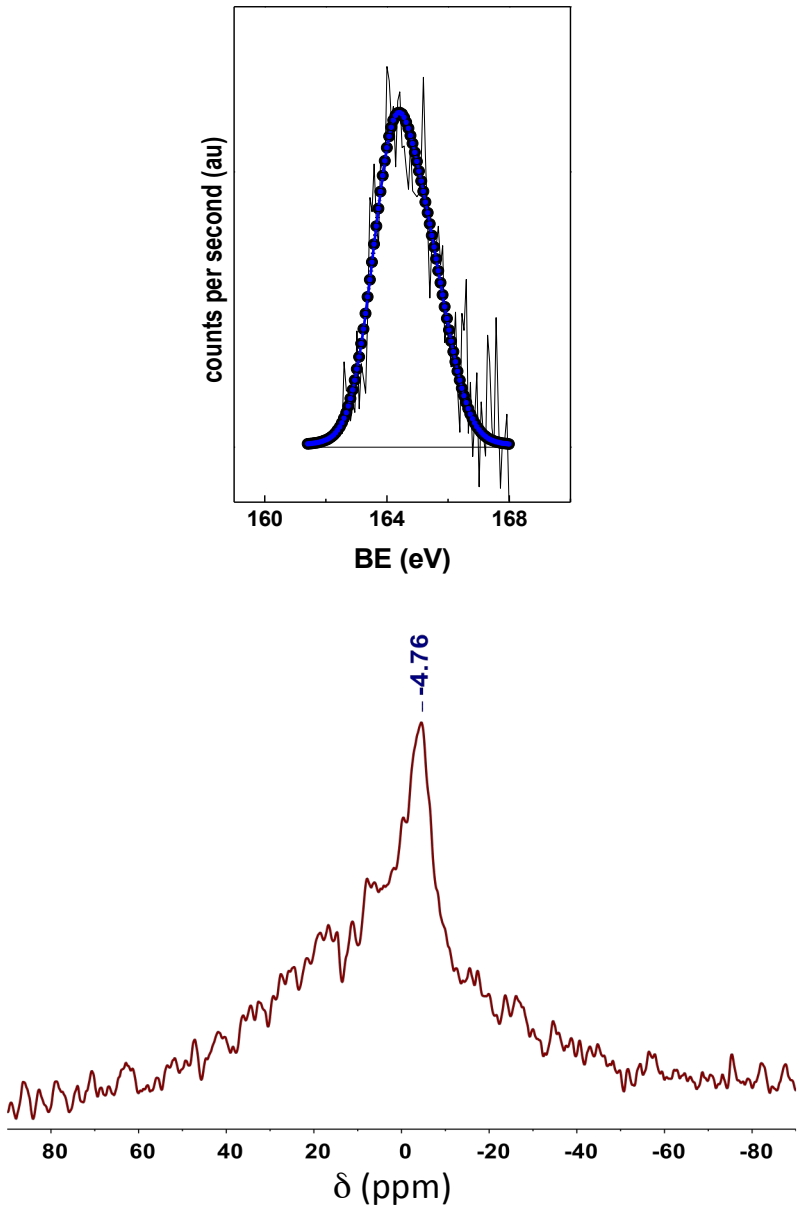

Figure 5. (a) Picture of the two monoliths of 12 mm in diameter and 1.5 mm in height assembled into the supercapacitor cell. (b) Voltammogram of P-doped carbon-CNT composites recorded at 5 mVs^{-1} for voltages of up to 1.5 V. (c) Specific capacitance measured for P-doped carbon-CNT composites. (d) CP charge-discharge curves of P-doped carbon-CNT composites registered at 1 (black line), 2.5 (red line), 11.67 (Green line), and 25 A/g (blue line). (e) Plot representing the retention of the specific capacitance over more than 10000 cycles in heavy regime conditions (0-1.5 V, 2.5 $A\ g^{-1}$). (f) Ragone plot representing data obtained from a set of different monoliths; the P-doped carbon–CNT composite monolith of 12 mm in diameter and 1.5 mm in height described herein (solid circles), a non-doped carbon–CNT composite monolith of 12 mm in diameter and 1.0 mm in height described in Ref. 68 (solid squares), a P-doped carbon monolith of 10 mm in diameter and 1.4 mm in height described in Ref. 67 (solid diamonds), and a non-doped carbon monolith of 11 mm in diameter and 1.8 mm in height described in Ref. 17 (solid triangles). (g) Picture of a IR LED – with a threshold voltage of 1.4 V and a power consumption of 30 mW – emitting light when connected to the supercapacitor cell built up with two monoliths of 12 mm in diameter and 1.5 mm in height as electrodes.

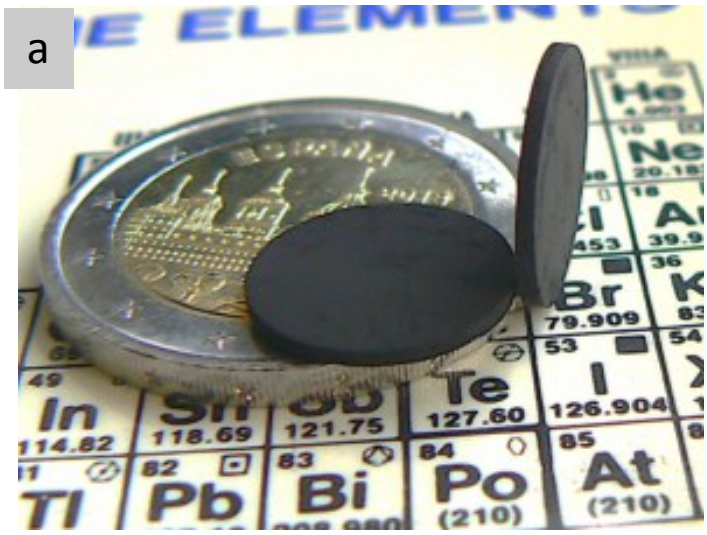

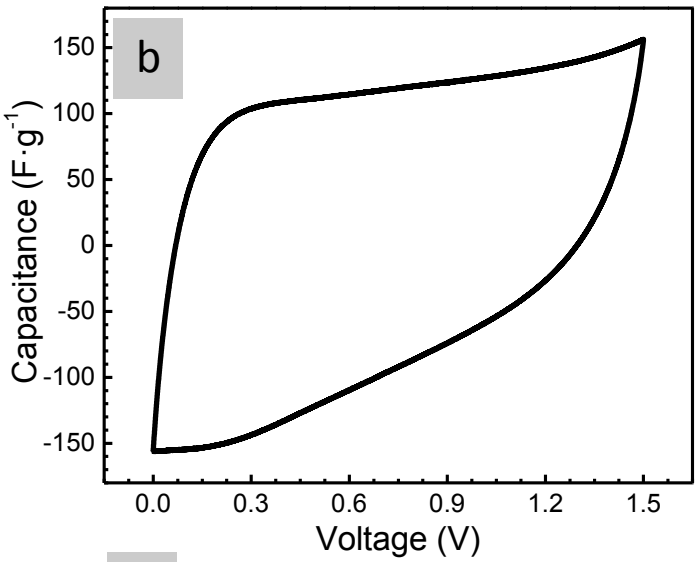

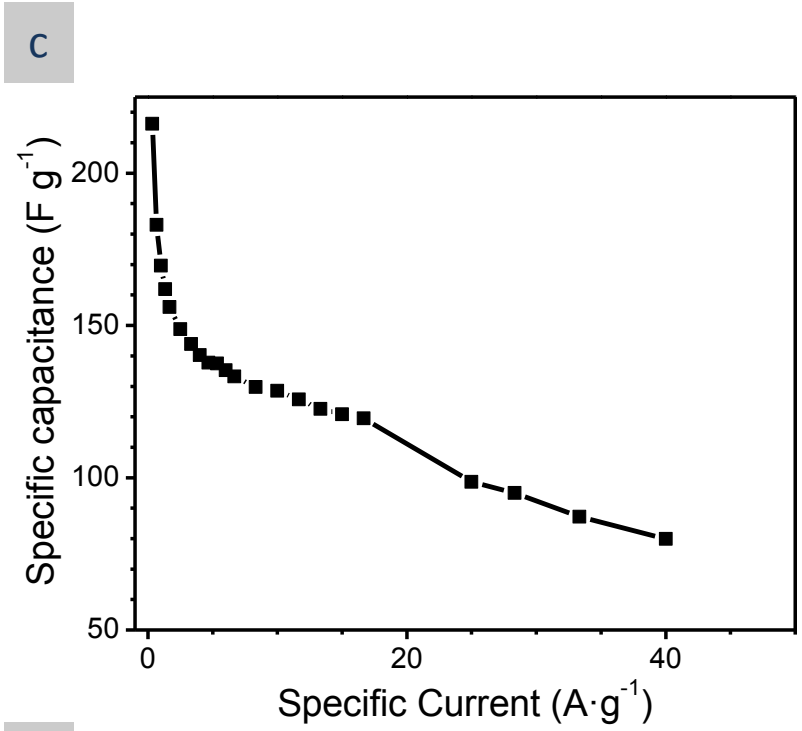

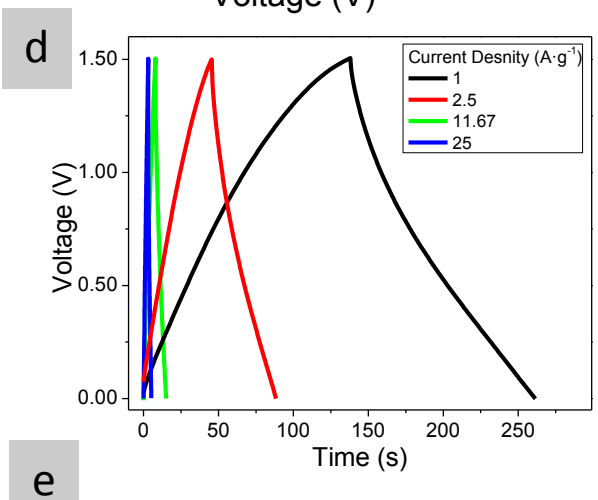

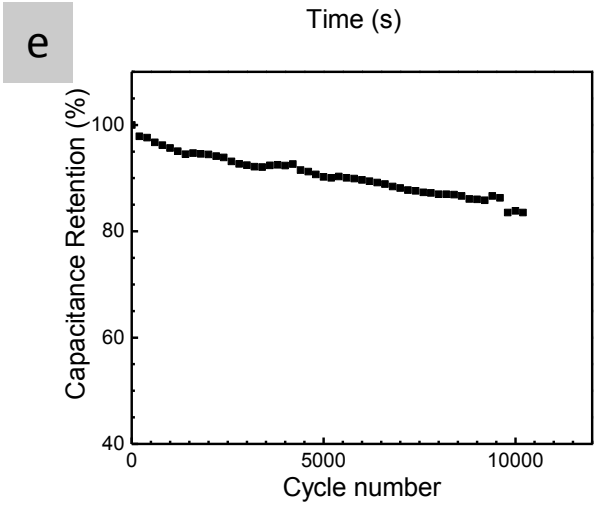

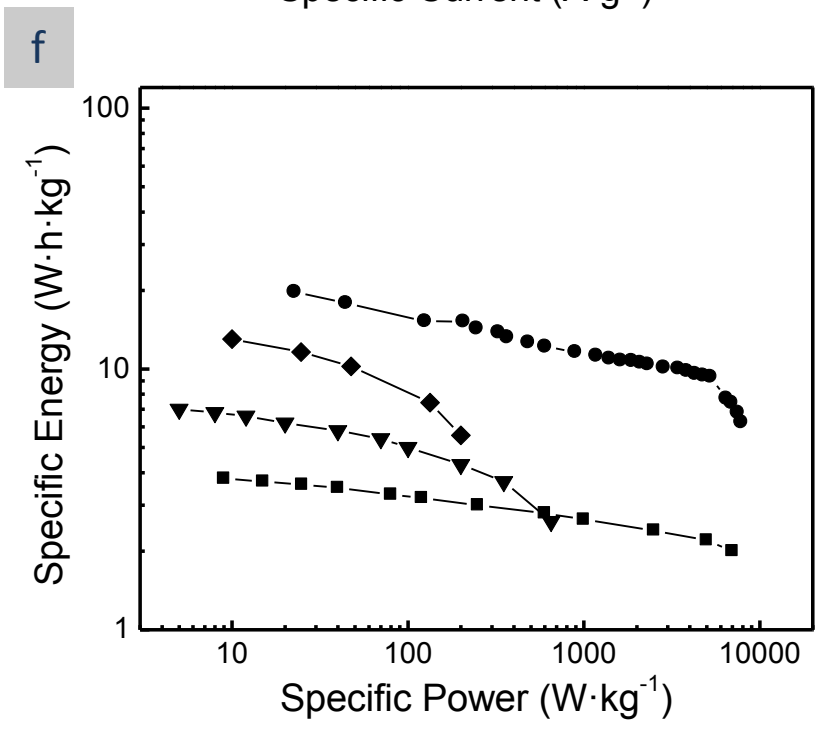

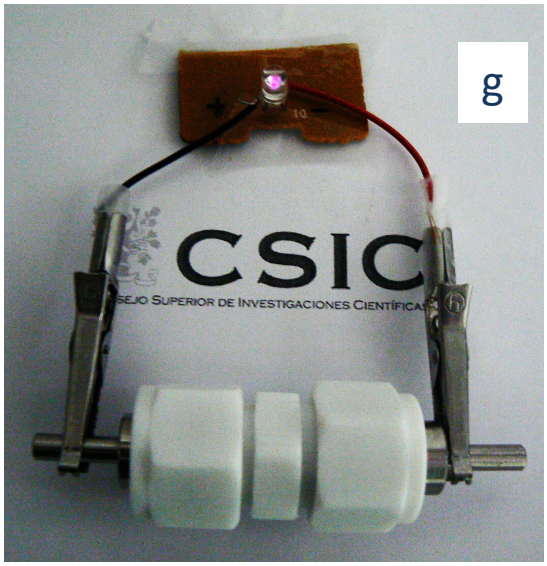

Figure 6. Nyquist (a) and Bode (b) plots of P-doped carbon-CNT composites obtained at different potentials for frequencies ranging from 0.01 to 10^5 Hz and an amplitude of 10mV.

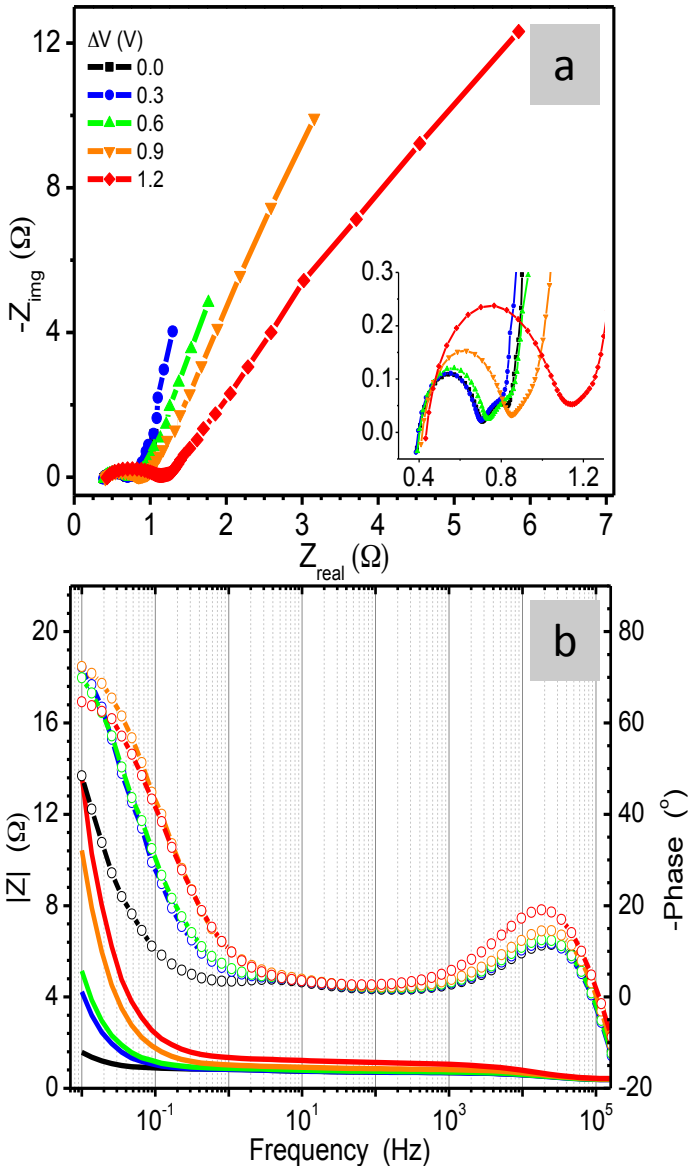

TOC text

Phosphorus-doped carbon-carbon nanotube hierarchical monoliths exhibiting energy densities of around 22.6 W h kg^{-1} at power densities of up to 10 kW kg^{-1} were capable to work as true three-dimensional electrodes in supercapacitor cells

TOC graphic